Powder Metallurgy and Metal Ceramics, Vol. 50, Nos. 1-2, May, 2011 (Russian Original Vol. 50, Nos. 1-2, Jan.-Feb., 2011)

PROCESSING AND PROPERTIES OF HIGHLY POROUS 17-4 PH STAINLESS STEEL

I. Mutlu,[1,2] E. Oktay[1]

UDC 621.762:621.793.79

Highly porous 17-4 PH stainless steel having porosities in the range of 39–82% with an average pore size of around 700 μm was successfully fabricated using space holder technique in powder metallurgy. Irregular carbamide particles were used as a space holder material. The final porosity was directly related to the added fraction of carbamide. The specimens were sintered at either 1300°C or 1350°C for times of 60 and 90 min in hydrogen atmosphere. In this porosity range, Young's modulus and compressive strength of the specimens before aging treatment found to be in the range of 0.17–5.34 GPa and 24–290 MPa, respectively and decreased with increasing porosity. 0.5 wt.% boron addition to the 17-4 PH steel powders lowered the sintering temperature and time. The relationship between the mechanical properties and the relative density of porous 17-4 PH steel was found to obey the power law relation.

Keywords*: porous materials, powder metallurgy, space holder, 17-4 PH stainless steel, sintering.*

INTRODUCTION

Highly porous metals can have open-cell and closed-cell structures which make them useful for many engineering fields. Porous metals having predominantly closed-cell pore structure are being used in lightweight constructions, mechanical energy and sound absorption. Moreover their thermal conductivity is low. Open cell structure makes them most useful for heat exchangers, filters, membranes and catalyst carriers [1–4]. In particular, highly porous stainless steel, titanium and superalloy based materials with open cell structures have been acknowledged as biomaterials for use in biomedical applications. Their porous structures are not only biocompatible but also allow body tissues to grow inside and body fluids to be transported through the interconnected pores, thus accelerating the healing process [2, 5–9].

A variety of methods are available to produce porous metals with a volume fraction of pores in the range of 5–80%. Through a process of casting [1, 3], sputter deposition [1] and powder metallurgy [2, 5, 6], porous materials with large pores (200 μm to 2 mm) can be produced. The powder metallurgy process was proved to be the most economic, feasible and promising technique in manufacturing of porous metal parts. Space holder and sintering technique in powder metallurgy process has been used to manufacture highly porous metallic materials such as stainless steel, titanium and superalloys. The process is composed of four sequential steps: mixing of the metal powder with polymeric binder and space holder particles (pore former), compaction of the mixture to produce green body, removing the space holder by thermally or chemically from the green body and sintering. Several space

[1]Istanbul University, Metallurgical and Materials Engineering Department, Istanbul, Turkey; e-mail: imutlu@istanbul.edu.tr.

Published in Poroshkovaya Metallurgiya, Vol. 50, No. 1–2 (477), pp. 94–105, 2011. Original article submitted June 1, 2010.

holder agents have been used in the past, including salt, polymers, naphthalene, ammonium bicarbonate and carbamide. In the space holder and sintering technique, the crucial step is removal of the space holder from the green body [2, 5, 6, 10]. Thermal removal of the space holder takes a long time since a slow heating rate is required to obtain crack free specimens. In addition, decomposition of the space holder material releases harmful gas species that may also interact with the metal.

Bakan [6] introduced a water leaching method to remove the carbamide from 316L stainless steel green compacts in water. Later, Tuncer and Arslan [10], and Gulsoy and German [11] removed carbamide from green specimens using the same method. This method is especially attractive because water is non-toxic and non-flammable. Furthermore, the use of water as a leaching medium eliminates the environmental drawbacks related to the removal of organic space holders. As an additional benefit, the equipment necessary for water leaching is very simple.

Precipitation hardenable 17-4 PH martenstic stainless steel combines good corrosion resistance with sufficient strength that is higher than conventional AISI 316 steel. In addition its mechanical properties can be improved by precipitation hardening heat treatment. Recently, Gulsoy and German [10] manufactured porous 17-4 PH stainless steel specimens having porosities 40, 50 and 60% by space holder-sintering technique and determined the compressive strength and elastic moduli of the porous specimens after precipitation hardening. They found that the specimen with 60% porosity had Young's modulus of 46 GPa and compressive yield stress of 834 MPa. However, there is no study on 17-PH steel having porosities greater than 60% in the literature. Also, effects of boron addition on the mechanical properties of highly porous 17-PH steel have not been reported in detail.

In this study, highly porous 17-4 PH stainless steel specimens having different levels of porosities (39–82%) were produced using space holder-sintering technique. The specimens were compressively tested before the precipitation hardening heat treatment in order to obtain a better understanding of compressive behaviours. In addition, effects of boron addition on the sintered properties of highly porous 17-4 PH stainless steel were investigated.

EXPERIMENTAL

In this study, gas atomised spherical 17-4 PH stainless steel powder (obtained from Carpenter Powder Products, Sweden) was used. Figure 1 shows scanning electron microscope (SEM), JEOL JSM 5600, image of the stainless steel powder. The chemical composition of the 17-4 PH stainless steel powder was Fe–(4.6% Ni, 15.2% Cr, 0.7% Mo, 0.4% Nb, 4.9% Cu, 1.4% Si). Particle size distribution of the 17-4 PH stainless steel powder was determined by using a Malvern Mastersizer 2000 analyser and given in Fig. 2. The cumulative size distribution at the 10, 50 and 90 percentiles corresponds to particle sizes of D_{10} = 6.9 μm, D_{50} = 14.7 μm, and D_{90} = 26.9 μm. Apparent, tap and pycnometer densities of the stainless steel powder were determined to be 3.59, 4.44, and 7.81 g · cm^{-3}, respectively.

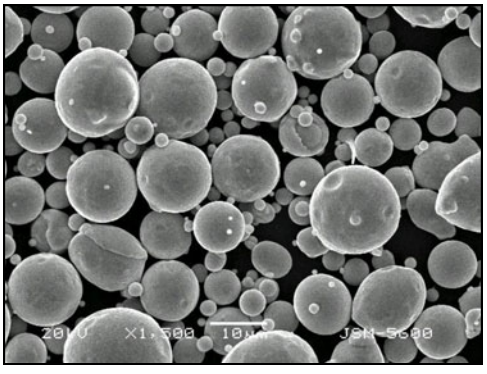

Fig. 1. SEM image of the 17-4 PH stainless steel powders

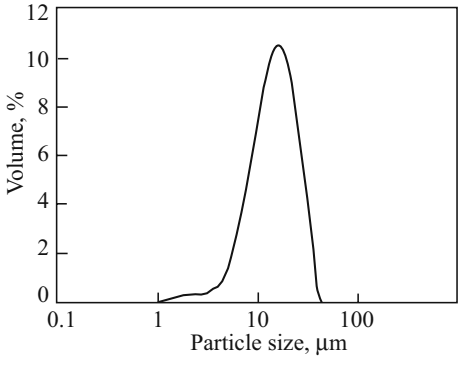

Fig. 2. Particle size distribution of the 17-4 PH stainless steel powder

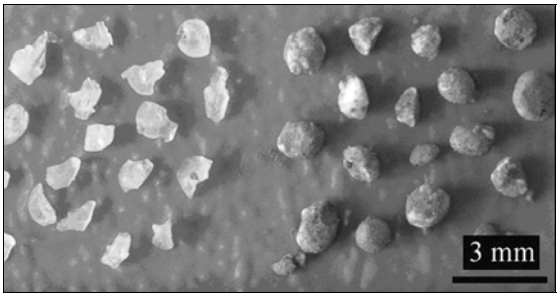

Fig. 3. Irregular shaped carbamide particles (left) and covered carbamide particles (right)

As a space holder material, carbamide, also named urea, was chosen for its advantage of ease of removal in water. Spherical carbamide particles (supplied by Merck KGaA, Germany) had a density of 1.34 $g \cdot cm^{-3}$, melting temperature of 133°C, and solubility in water at 20°C of more than 1000 $g \cdot L^{-1}$. As received spherical carbamide particles were crushed and sieved to obtain the fraction of 710–1000 μm with an irregular shape. Experiments were carried out with irregular shaped carbamide in order to increase the packing efficiency. The weight ratios of the steel powder to the amount of carbamide were calculated to obtain defined porosities in the range of 40–80% in the sintered specimens.

The binder ingredient for green strength was paraffin wax, supplied by Merck KGaA, Germany, with a melting range of 46–48°C. It was used at 4 wt.% based on the 17-4 PH stainless steel mass. The 17-4 PH stainless steel powder was first mixed manually with hot paraffin wax solution. This mixing process was necessary because all the steel powder must be covered with the binder. Carbamide was moistened with distilled water to form sticky surface and then waxed stainless steel powder was added. Mixing of the stainless steel and carbamide powders was performed in a Turbula mixer, which traces a three-dimensional ‘‘figure of eight’’ motion, for 45 min. As a result the steel powder particles adhered to the surface of the carbamide particles. Figure 3 shows uncovered irregular shaped carbamide particles (left) and carbamide particles covered with the 17-4 PH steel powder (right). A homogeneous coating of the carbamide particles with the steel powder was obtained as it is seen in Fig. 3.

The covered carbamide particles then compacted uniaxially at 180 MPa in a steel die using a hydraulic press into cylindrical specimens with a diameter of 12 mm and heights of 17–20 mm. In order to determine the optimum compaction pressure, a series of compaction experiments were carried out by varying the pressure from 100 to 500 MPa. Pressures higher than 180 MPa broke the carbamide particles thus changed the designed pore size and morphology. On the other hand specimens compacted at compaction pressures below 180 MPa could not remain their shape after removal of the carbamide in water. In view of these facts, optimum compaction pressure leading to a sound product is determined as 180 MPa for the 17-4 PH steel containing carbamide as space-holder.

The green specimens were immersed in distilled water at room temperature to leach the carbamide. Specimens were removed from the water at regular intervals, dried in air at 40°C and weighed. About 90% of the carbamide was leached out in 4 hours, as confirmed by weighing the specimens before and after the space holder removal step. A highly porous structure was achieved throughout the green specimens by performing water leaching of carbamide at room temperature.

Thermal debinding temperature of the paraffin wax was determined by using thermogravimetric analysis (TA Instruments, SDT Q600, DSC/TGA device) at a constant heating rate of 5°C under N_2 atmosphere. The starting sample amount was 28.7 mg. Figure 4 shows the thermogravimetric analysis (TGA) curve of the paraffin wax. TGA results showed that weight loss begun at 200°C and completed at 330°C.

The paraffin wax in the green specimens was thermally removed as part of sintering cycle, which consisted of heating at a ramp rate of 5°C $\cdot$ min^{-1} to 380°C with a dwell time of 40 min (debinding stage), followed by heating at rate of 10°C $\cdot$ min^{-1} to sintering temperatures. The specimens were sintered at either 1300°C or 1350°C for times of 60 and 90 min. The sintering cycle was performed in high purity hydrogen in a horizontal tube furnace (Lenton, UK). Furnace was purged with N_2 gas before the sintering process.

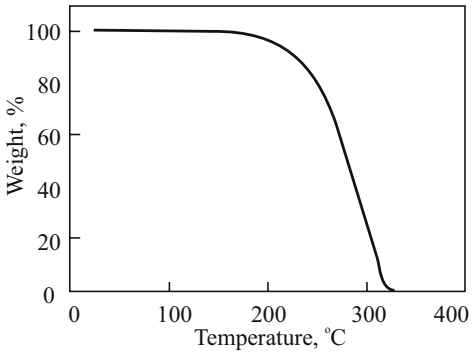

Fig. 4. TGA curve of the paraffin wax

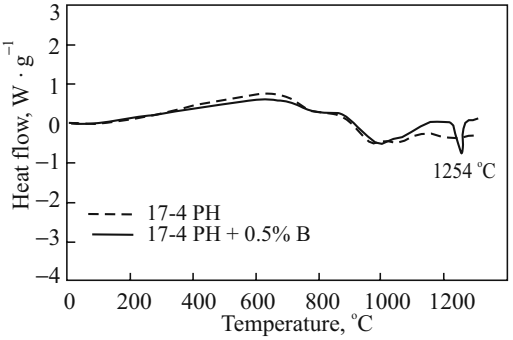

Fig. 5. DSC curves

In addition, boron was used as a liquid phase additive for sintering of the 17-4 PH stainless steel powder. For this purpose, 17-4 PH stainless steel powder were mixed with 0.5 wt.% amorphous boron powder, $D_{50} = 2$ μm, supplied by Merck KGaA (Germany). Then, the same standard process was carried out for the powder mixtures containing boron.

The effect of boron addition on the liquid formation temperature of the 17-4 PH steel was determined by using differential thermal analysis (TA Instruments, SDT Q600, DSC/TGA device). The differential thermal analysis was performed at a constant heating rate of 5°C · min^{-1} under argon atmosphere. The starting sample amount was 50.1 mg. Figure 5 shows DTA curves of the 17-4 PH steel powder and 0.5 wt.% boron added 17-4 PH steel powder. Sample containing 0.5 wt.% boron shows an endothermic peak at 1254°C in the DTA curve indicating liquid formation. The other peaks observed on the curves are due to polymorphic transformation of the steel. Thus specimens containing boron were sintered at a temperature of 1260°C. The boron-containing specimens were sintered at this temperature for 40 min.

Densities of the sintered specimens were determined from measurements of weights and dimensions of the specimens. The microstructures and pore morphology of the highly porous stainless steel specimens were examined by scanning electron microscopy (SEM). Pore size, pore size distribution and pore shape were determined by quantitative image analyses using commercial image analyser software, Clemex Vision Professional Edition, version 4.0.021c. The area of each pore on the SEM image was calculated, and then spherical diameter as pore size and sphericity as pore shape were computed.

Mechanical properties of the specimens were studied by the compression test performed on a Zwick-Roell Z050 materials testing machine. Compression tests were carried out at a crosshead speed of 0.5 mm · min^{-1}. At least three specimens were tested under the same conditions to assess repeatability. The stress was calculated using the apparent cross-sectional area of the respective specimen, after which Young's modulus for each specimen was determined from the slope of the corresponding stress-strain graph.

RESULTS

17-4 PH stainless steel specimens with porosities ranging between 39% and 82% were successfully produced. The pore shape replicated the initial shape of the carbamide powder particles that were used to produce the green compact. Sintered density varied with the added fraction of space holder material in the initial formulation. As the carbamide powder content increased, the sintered density decreased and the porosity increased in all specimens. Figure 6 shows the sintered specimens having 71 and 82 vol.% porosity.

SEM images of the surfaces of sintered specimens having different porosities are provided in Fig. 7 and show a relatively uniform distribution of pores. No cracks were observed in the porous structures. In spite of sintering between the stainless steel particles, the macropore framework remained with a small shrinkage. In all specimens, morphology of the final pores was similar to that of the carbamide powder particles. This suggests that pore structures can be designed by using proper size, shape and content of carbamide particles.

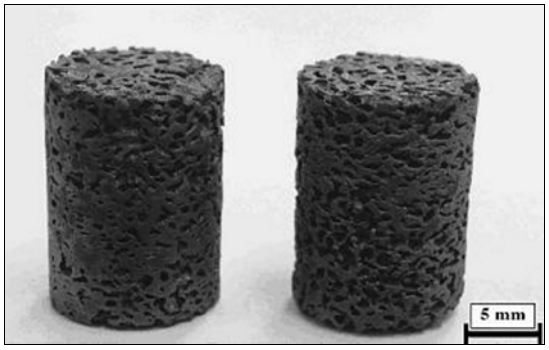

Fig. 6. Sintered 17-4 PH steel specimens having 71% porosity (left) and 82% porosity (right)

Figure 8 shows SEM images of the boron free and boron added porous 17-4 PH steel specimens. As it can be seen from Fig. 8a, micropores existed in the boron-free specimens because of insufficient solid state sintering. However, micropores were mostly eliminated in the specimen containing boron as shown in Fig. 8b. The binary Fe–B phase diagram shows the existence of the intermetallic Fe_2B, which forms an iron-rich low melting eutectic at about 1174°C and ~4 wt.% boron [12]. The DTA curve of 0.5% boron containing 17-4 PH steel given in Fig. 5 also revealed that the formation of the liquid phase. The liquid phase has a very low solubility in iron and remains as an almost continuous network between solid grains, favouring the classical phenomenon of the liquid phase sintering [12, 13]. The increase in the eutectic temperature for 17-4 PH is attributed to the presence of substitutional elements like Cr and Mo. Sintering of boron added specimens were carried out at 1260°C temperature and time of 40 min, which was considerably lower than that of boron-free specimens. The microporosity in the sintered specimens should be kept as low as possible if a high strength porous metal solid is desired. Micropores decrease the mechanical properties by reducing the load bearing cross-sectional area of the pore walls.

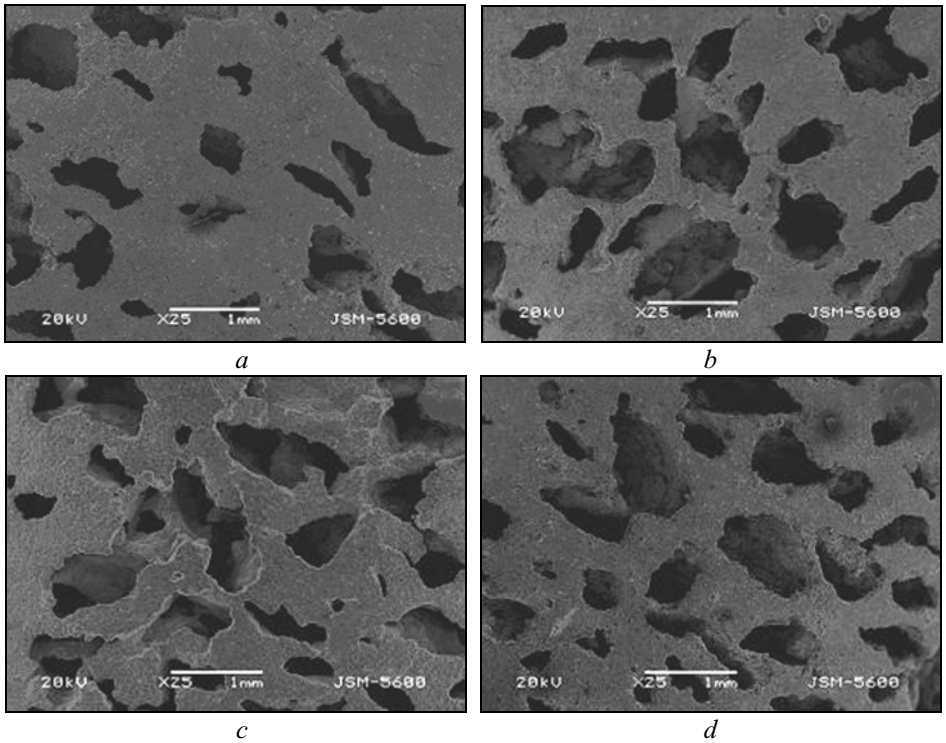

a *b*

c *d*

Fig. 7. SEM images of the highly porous 17-4 PH steel specimens having (*a*) 50, (*b*) 62, (*c*) 71, and (d) 82% porosity

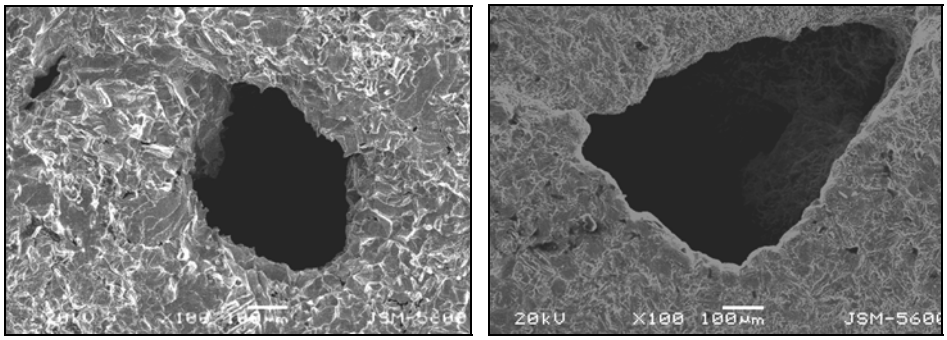

a *b*

Fig. 8. SEM images of the porous 17-4 PH steel specimens (*a*) without boron addition, sintered at 1350°C for 60 min (*b*), with 0.5 wt.% boron addition, sintered at 1260°C for 40 min

The SEM images of the porous specimens were also used to determine the mean pore size, pore distribution and pore shape by the image analyser software. The area of each pore was calculated on the SEM image, and equivalent spherical diameter as pore size and sphericity as pore shape was computed.

Figure 9 shows pore size distribution in terms of spherical diameter of a 71% porous specimen. Mean, maximum and minimum pore size values of the pores are 692, 254 and 1369 μm, respectively. The observed pore sizes above 1000 μm indicate the amount of pore coalescence, which corresponds to about 15% of the total pores. In addition, about 80% of the pores have the pore size in the range of 500–1000 μm. Pore morphology (shape) is also investigated by the image analyser in terms of the sphericity value. Figure 10 shows the sphericity distribution of the pores for 71% porous specimen; it can be seen that about 92% of the pores have sphericity values higher than 0.3 with an average of 0.57 sphericity. Sphericity of the carbamide particles was determined to be 0.63.

The compressive stress–strain curves of boron free and boron added 17-4 PH stainless steel specimens fabricated by the space holder method with different porosities are illustrated in Fig. 11, 12. Three distinct regions characterized the curves; an elastic region at an initial stage where cell walls bending occur; a large plateau region with nearly constant flow stress to large strains where cell walls buckle, yield and fracture and a densification region where the flow stress rapidly increases. The stress, after a first maximum, drops significantly as a result of

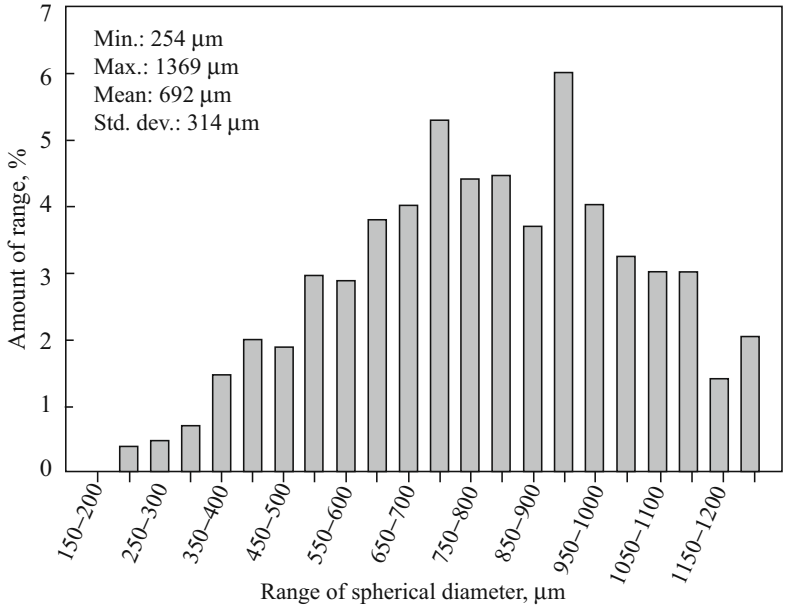

Fig. 9. Spherical diameter (pore size) distribution of 71% porous specimens produced using irregular carbamide particles

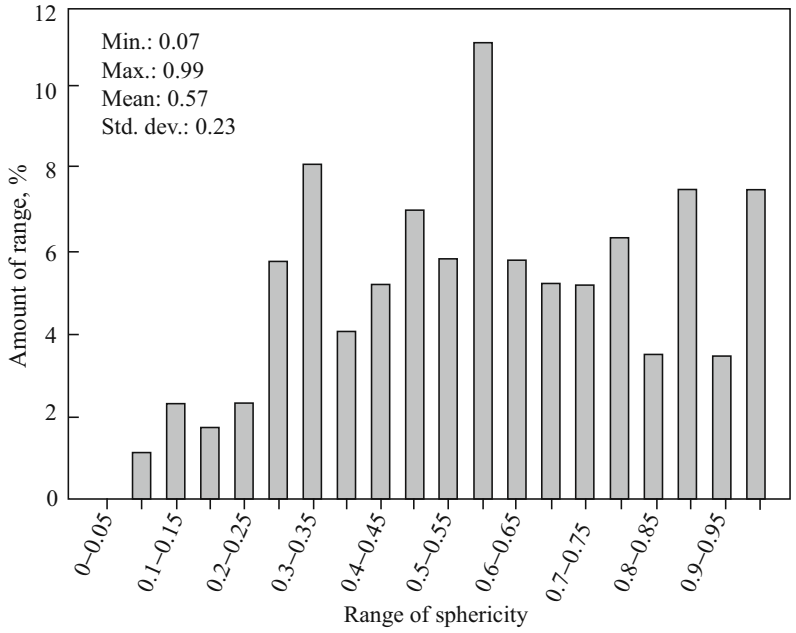

Fig. 10. Sphericity distribution of 71% porous specimens produced using irregular carbamide particles

the collapse of a pore layer. Once the cell edge collapses at the yield point of the solid, the collapsed edge has little ability to bear the load and bends easily by a low stress.

The deformation mode, resulting from the abrupt and repeatable failure of the successive pore layers, gives rise to very uneven character of the stress-strain curve. The deformed structure exhibited extensive cell wall failures. At the end of the plateau region, stress starts to increase since the pores at the deformation zone have flattened and the material attains bulk-like properties under compression. Compression tests of the porous 17-4 PH steel specimens showed that the compressive strength values (the first maximum of the deformation curves) decreased and length of the plateau region increased with increasing porosity content. Long plateau regions with nearly constant flow stresses to large strains are an indication of open cellular morphology. Compressive yield strength values of boron free specimens containing porosities in the range 39–80% were observed to vary between 24–270 MPa. The resultant elastic moduli were between 0.83–5.34 GPa. Compressive yield strength values of 0.5 wt.% boron containing specimens with porosities in the range 42–82% were between 38–290 MPa and the elastic moduli were between 0.17–4.82 GPa.

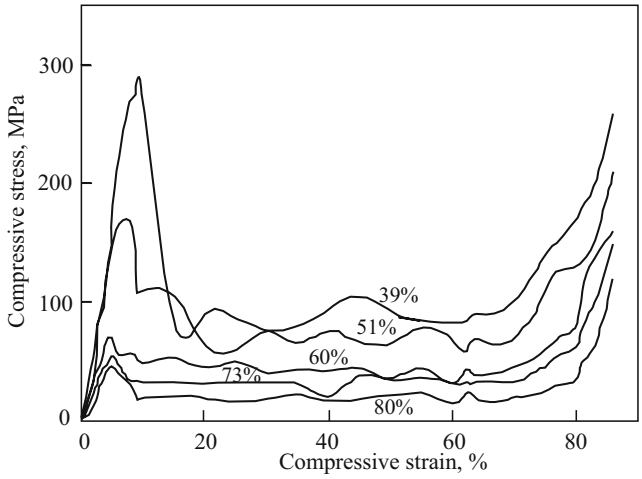

Fig. 11. Compressive stress–compressive strain curves of the boron-free 17-4 PH steel specimens, sintered at 1350°C for 90 min, having different porosities

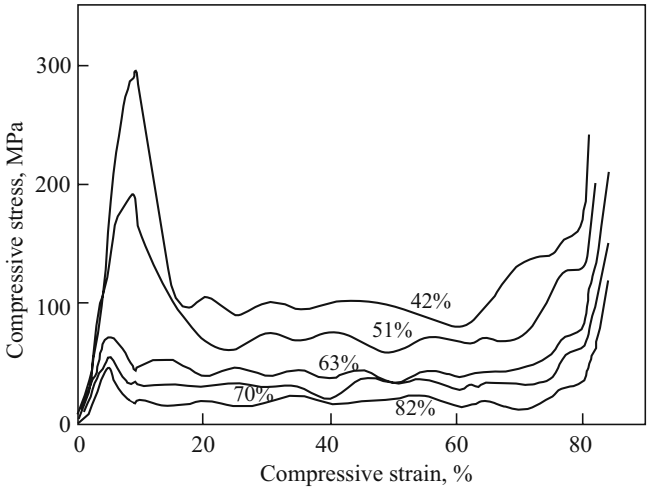

Fig. 12. Compressive stress–compressive strain curves of the boron added 17-4 PH specimens, sintered at 1260°C for 40 min, having different porosities

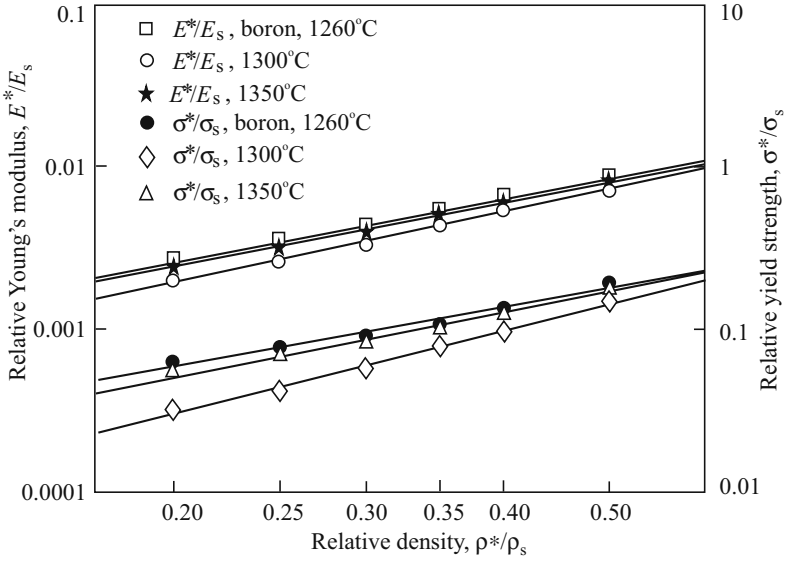

Fig. 13. Change of relative yield stress and relative Young's modulus with relative density of the boron added and boron free 17-4 PH steel specimens

Gibson and Ashby [14], proposed a model to express the mechanical properties of porous materials. The Gibson and Ashby model assumes the pore walls as solid metal and finds that the contribution of cell face stretching to the overall stiffness and strength of the foam is linearly dependent on the relative density while the contribution of cell edge bending is nonlinear. However, this model is valid to metal foams with a porosity of 70% or higher.

In this study, the data of relative compressive yield strength and relative Young's modulus of the porous 17-4 PH steel specimens were plotted against the relative density as shown in Fig. 13, and given rise to the equations (1) and (2) for boron free specimens sintered at 1300°C:

$$\left(\frac{E*}{E_s}\right) = 0.02\left(\frac{\rho*}{\rho_s}\right)^{1.45} \quad (R^2 = 0.94), \tag{1}$$

$$\left(\frac{\sigma*}{\sigma_s}\right) = 0.47\left(\frac{\rho*}{\rho_s}\right)^{1.69} \quad (R^2 = 0.92), \tag{2}$$

equations (3) and (4) for boron free specimens sintered at 1350°C:

$$\left(\frac{E^*}{E_s}\right) = 0.03\left(\frac{\rho^*}{\rho_s}\right)^{1.79} \quad (R^2 = 0.97), \tag{3}$$

$$\left(\frac{\sigma^*}{\sigma_s}\right) = 0.44\left(\frac{\rho^*}{\rho_s}\right)^{1.68} \quad (R^2 = 0.96), \tag{4}$$

and equations (5) and (6) for boron containing specimens sintered at 1260°C:

$$\left(\frac{E^*}{E_s}\right) = 0.02\left(\frac{\rho^*}{\rho_s}\right)^{1.22} \quad (R^2 = 0.94), \tag{5}$$

$$\left(\frac{\sigma^*}{\sigma_s}\right) = 0.41\left(\frac{\rho^*}{\rho_s}\right)^{1.26} \quad (R^2 = 0.94), \tag{6}$$

where σ^*, E^*, and ρ^* are the compressive yield strength (the first peak of the deformation curve), Young's modulus and density of the porous specimens respectively, while σ_s, E_s, and ρ_s are the corresponding properties of the bulk 17-4 PH steel. The density, yield strength and Young's modulus of the bulk 17-4 PH steel are 7.85 $g \cdot cm^{-3}$, 960 MPa and 194 GPa, respectively. The linear relationships are fairly good ($R^2 > 0.92$) for the equations. It is clear that the relative density (porosity content) mainly affects the yield strength and Young's modulus of the porous 17-4 PH steel. The proportionality constant and the exponent values reflect to foam characteristics, such as cell morphology, shape and arrangement of cell walls. Imperfections, such as broken walls, large pores, anisotropic pore structure and non-uniform foam density and micropores in cell walls significantly affect the mechanical properties of the cellular solids produced by powder metallurgy. Micropores decrease the mechanical properties by reducing the load bearing cross-sectional area of the pore walls. Higher sintering temperatures, longer times and sintering additives that cause liquid phase sintering are required to reduce the microporosity of sintered powder compacts. A positive effect of boron via liquid phase sintering gave rise densification of cell walls. This was caused an increase of the relative compressive strengths of porous steel specimens as shown in Fig. 11. Increasing the sintering time and temperature also help densification of the cell walls that results increases in the relative compressive strengths of porous steel specimens as shown in Fig. 12.

The relative compressive strengths of porous boron free steel specimens sintered at 1350°C for 90 min had relative compressive strength values close to the porous steel specimens containing boron that were sintered at 1260°C for 40 min. Also, microstructural study on the cell walls revealed that micro porosity is reduced by liquid phase sintering as shown in Fig. 8.

CONCLUSIONS

Highly porous 17-4 PH stainless steel having porosities in the range of 39–82% with an average pore size of around 700 μm was successfully fabricated using the space holder technique in powder metallurgy. The macropores remained nearly unchanged after the sintering process. The final porosity is directly related to the added fraction of carbamide.

Pore shape was similar to initial carbamide particle shape. These findings suggest that selecting an appropriate carbamide particle type can control morphology of the pores. It is also possible to obtain a tailored pore size distribution in the highly porous specimens by using carbamide having a different particle size range. In this porosity range, Young's modulus and compressive strength of the specimens before aging treatment found to be in the range of 0.17–5.34 GPa and 24–290 MPa, respectively and decreased with increasing porosity. Long plateau regions with nearly constant flow stresses to large strains are an indication of open cellular morphology.

Boron addition (0.5 wt.%) to the 17-4 PH steel powders lowered the sintering temperature and time. Increasing sintering temperature, sintering time and addition of boron enhanced the mechanical properties of highly

porous 17-4 PH steel. The relationship between the mechanical properties and the relative density of porous 17-4 PH steel was found to obey a power law relation.

ACKNOWLEDGEMENT

This work was supported by Scientific Research Projects Coordination Unit of Istanbul University, Project number T-1430.

REFERENCES

1. M. F. Ashby, A. Evans, N. A. Fleck, et al., *Metal Foams: A Design Guide*, Elsevier Science, Boston, MA (2000).
2. M. Bram, C. Stiller, H. P. Buckramed, et al., "High-porosity titanium, stainless steel, and superalloy parts," *Advanced Engineering Materials*, **2**, No. 4, 196–199 (2000).
3. J. Banhart, "Manufacture, characterisation and application of cellular metals and metal foams," *Progress in Materials Science*, Vol. **46**, No. 6, 559–632 (2001).
4. H. P. Degisher, B. Kriszt, *Handbook of Cellular Metals*, Wiley-VCH, Weinheim (2002), p. 313.
5. W. Niu, C. Bai, G. Qiu, Q. Wang, "Processing and properties of porous titanium using space holder technique," *Materials Science and Engineering A*, No. 506, 148–151 (2009).
6. H. I. Bakan, "A Novel water leaching and sintering process for manufacturing highly porous stainless steel," *Scripta Materialia*, **55**, 203–206 (2006).
7. A. Laptev, M. Bram, H. P. Buchkremer, D. Stover, "Study of production route for titanium parts combining very high porosity and complex shape," *Powder Metallurgy*, **47**, 85–92 (2004).
8. D. C. Dunand, "*Adv. Eng. Mater*.," No. 6, 369 (2004).
9. C. E. Wen, M. Mabuchi, Y. Yamada, "Processing of biocompatible porous Ti and Mg," *Scripta Materialia*, **45**, 1147–1153 (2001).
10. N. Tuncer, G. Arslan, "Designing compressive properties of titanium foams," *J. Mater Sci*., **44**, 1477–1484 (2009).
11. H. O. Gulsoy, R. M. German, "Sintered foams from precipitation hardened stainless steel powder," *Powder Metallurgy*, **51**, No. 4 (2008).
12. H. O. Gulsoy, S. Salman, S. Ozbek, F. Findik, "Sintering of a Boron-doped injection moulded 17-4 PH stanless steel," *J. Mater Sci.*, **40**, 4101–4104 (2005).
13. *H. I. Bakan, D. Heaney, R. M. German*, "Effect of Nickel Boride and Boron additions on sintering characteristics of injection moulded 316L powder using water soluble binder system," *Powder Metallurgy*, **44**, No. 3, 235–242, (2001).
14. L. J. Gibson, M. F. Ashby, *Cellular Solids–Structures and Properties*, University Press, Cambridge (1997).